1   **LiDAR simulation in modelled orchards to optimise the use of**

2   **terrestrial laser scanners and derived vegetative measures**

3

4   Valeriano Méndez[a, c, d], Heliodoro Catalán[a], Joan R. Rosell-Polo[b], Jaume Arnó[b], Ricardo

5   Sanz[b]

6

7   [a]Department of Applied Mathematics. Polytechnic University of Madrid. Ciudad

8   Universitaria, s/n, 28040 Madrid, Spain.

9

10   [b]Department of Agricultural and Forest Engineering. University of Lleida. Rovira

11   Roure, 191, 25198 Lleida, Spain.

12

13   [c]Corresponding author. Tel.: +34 917 308 355. E-mail: valeriano.mendez@upm.es

14

15   [d]Proofs correspondence. Valeriano Méndez. Department of Applied Mathematics.

16   E.T.S. Ingenieros Agrónomos. Polytechnic University of Madrid. Ciudad Universitaria,

17   s/n, 28040 Madrid, Spain.

18

19

20   *ABSTRACT*

21   Light detection and ranging (LiDAR) technology is beginning to have an impact on

22   agriculture. Canopy volume and/or fruit tree leaf area can be estimated using terrestrial

23   laser sensors based on this technology. However, the use of these devices may have

24   different options depending on the resolution and scanning mode. As a consequence,

25   data accuracy and LiDAR derived parameters are affected by sensor configuration, and

26　may vary according to vegetative characteristics of tree crops. Given this scenario, users

27　and suppliers of these devices need to know how to use the sensor in each case. This

28　paper presents a computer program to determine the best configuration, allowing

29　simulation and evaluation of different LiDAR configurations in various tree structures

30　(or training systems). The ultimate goal is to optimise the use of laser scanners in field

31　operations. The software presented generates a virtual orchard, and then allows the

32　scanning simulation with a laser sensor. Trees are created using a hidden Markov tree

33　(HMT) model. Varying the foliar structure of the orchard the LiDAR simulation was

34　applied to twenty different artificially created orchards with or without leaves from two

35　positions (lateral and zenith). To validate the laser sensor configuration, leaf surface of

36　simulated trees was compared with the parameters obtained by LiDAR measurements:

37　the impacted leaf area, the impacted total area (leaves and wood), and the impacted area

38　in the three outer layers of leaves.

39

43

Variable	Description
+	Branching morphologic function. A shoot in a new axis is created by sympodial bud growth.
>	Succession morphologic function. A new shoot is created by apical bud growth.
α	Angle used in a turn geometric operation (degrees).
β	Polar angle used in shady process (degrees).
$\mathbf{d}, \mathbf{d}_2$	A direction in a vertex used for apical or sympodial growth.
$\Delta\theta$	Angle increase between two different laser beams (°).
Δy	Distance increase in the advance of the tractor (mm).
F	Floral state, which results from floral differentiation of the apical meristem
GU	Growth unit.
I_{3L}	3-external impacted leaf area (dm^2).
I_L	Impacted leaf area (dm^2).
I_T	Impacted total area (dm^2).
φ	Azimuth angle used in shady process (°).
L	Long state composed in general of 20 metamers.
L_A	Foliar area (dm^2).
l_{ij}	Measured distance (mm) where i = 1, …, N and j = 1, …, M, given that N is the number of different laser beams and M is the number of steps in the tractor route.
M	Medium state composed in general of 8 metamers.

Ni	Number of internodes.
n	A normal direction used in a turn geometric operation.
O	A point at the end of a branch where a bud is located, and where a geometric turn is calculated to get a new branching direction.
P	A position of the scan sensor from which a laser beam starts.
p_{ij}	Markov probability matrix.
θ	Angle of a particular sampling beam in the scan, separated by $\Delta\theta$ from the previous laser beam (°).
R	Lindenmayer's system production.
$\rho(u)$	A parent vertex in a Markov tree.
S	Short state composed of a single metamer.
Ta	Tree age.
u	A vertex in a Markov tree.
Ω	The alphabet of the L-system.
w	Initial axiom in an L-system.
x	The lateral distance from the scanner positioned in the inter-row (mm).
x_0	The distance from the laser to the orchard (mm).
y	Cross-sectional advance in the OY axis (mm).
z	Height coordinates in the model (mm).
z_0	The height of the laser above the ground (mm).

45

1. INTRODUCTION

47 The contactless and non-destructive geometrical and structural characterisation of plants

48 has been a subject of research both in forest and agriculture over recent years, with the

49 use of light detection and ranging (LiDAR) in agriculture being a relatively more recent

50 development. This interest is due to the fact that many fundamental properties and

51 environmental interactions of plants and crops are related to the geometrical structure of

52 their main components. In this context, several sensing techniques have been developed

53 while others are the subject of continued research. Of the latter, stereo vision and

54 LiDAR laser scanners are the most promising and complementary techniques from an

55 operational and practical use and from a real field conditions point of view (Rosell and

56 Sanz, 2012).

57

58 LiDAR is an increasingly used optical active remote sensing technique that measures

59 range and/or other information of a distant target. For this purpose, LiDAR systems

60 (LS) comprise a laser emitter, which sends a light beam that strikes the object of

61 interest, and a light detector that captures a portion of the radiation reflected by the

62 object. By means of electronically processing of the target's scattered light, LS can

63 determine the distance between the sensor and the object. Two different principles can

64 be used for the measurement of range: i) the measurement of the phase-shift between

65 the emitted and the reflected laser beam (Phase-shift LiDAR), and ii) the measurement

66 of the time elapsed between the emission of a laser pulse and its detection after being

67 scattered by the target (Time-of-flight LiDAR). Most LS usually work in scanning

68 mode, changing the light emitting direction within a plane thousands of times per

69 second and measuring the distance for each angular direction with great precision. The

70   measurement outputs are usually the three-dimensional (x, y, z) spatial coordinates of

71   each detected point (so-called point clouds) although some LS provide other

72   measurements such as the intensity of one or more reflected laser beams. The use of

73   appropriate post-processing algorithms makes it possible to describe and reconstruct the

74   structure of the trees with a high degree of accuracy (Rosell *et al.*, 2009a).

75

76   Many studies have focused on exploring the application of LS to characterise both

77   forest canopies (Lefsky *et al.*, 1999**;** Holmgren and Persson**,** 2004**;** Maltamo *et al.*,

78   2004**;** Parker *et al.*, 2004**;** Riaño *et al.*, 2004**;** Omasa *et al.*, 2007), and agricultural

79   crops. As regards the latter, the evaluation of vegetative parameters both in tree crops

80   (Tumbo *et al.*, 2002; Wei and Salyani, 2005) and in herbaceous crops (Saeys *et al.*,

81   2009; Ehlert *et al.*, 2010; Gebbers *et al.*, 2011), the obtaining of 3-D structure of trees

82   (Rosell *et al.*, 2009a), and the estimation of leaf area in fruit trees and vineyards

83   (Palacín *et al.*, 2007; Rosell *et al.*, 2009b; Arnó *et al.*, in press) are among the most

84   relevant application areas of interest.

85

86   Also, the application of plant protection products (PPP) in tree crops has recently

87   opened the opportunity for the application of different sensors and electronic control

88   devices on sprayers. For instance, through the use of ultrasonic sensors it is possible to

89   apply pesticide treatments distinguishing the presence or absence of trees. If in addition

90   a device that allows an online calculation of leaf area or volume for each tree detected is

91   incorporated to this technique, it is possible not only to apply in the right places, but

92   also vary dose with foliar area or volume (Gil *et al.*, 2007; Solanelles *et al.*, 2006).

93   However, although ultrasonic sensors allow variable application dosage adapted to the

94   canopy characteristics, the use of LiDAR sensors presents advantages given their higher

95   spatial resolution and measuring speed (Escolà *et al.* 2007; Llorens *et al.*, 2011). In fact,

96   in research studies related to the optimisation of pesticide treatments, Walklate *et al.*

97   (1997 and 2002) introduced a methodology to calculate several geometrical parameters

98   in apple trees based on the possibilities offered by LiDAR systems. . These authors

99   obtained their results through a probabilistic interpretation of the interaction of the light

100   emitted by the sensor with the plants.

101

102   Concerning the construction of virtual vegetation, the first method used to create

103   sophisticated plant topology was that of modular representation. Plants develop as

104   repetitions of certain types of components (Barthélémy *et al.*, 1991; Bell 1994; Harper

105   *et al.*, 1986). A modular representation can be developed using spatial, geometrical or

106   topological approaches. In geometric modular representation, plants are decomposed in

107   organs as leaves, fruits or internodes. This type of representation enables a precise

108   description of the plant to be obtained by studying the interaction between plants and

109   their microenvironment (Dauzat, 1993; Sinoquet *et al.*, 1998). Topologic modular

110   representation is a decomposition in which emphasis is placed on the connections

111   between organs. Several models of water flux in plants have been proposed based on an

112   electrical analogy (Dauzat *et al.*, 1999; de Reffye *et al.*, 1997; Früh, 1997). The

113   topologic model has been used to address carbon-partitioning problems. The modelling

114   of pipes, where every pipe is related to a leaf, is an example of topologic model

115   (Shinozaki *et al.*, 1964; Valentine, 1985). As computer calculation capacity has

116   expanded, plant growing simulation programs which utilise the topologic model have

117   been used to develop realistic three-dimensional models of the plant architecture

118   (Diggle, 1988; Fisher and Weeks, 1985; Ford *et al.*, 1990; Prusinkiewicz and

119   Lindenmayer, 1990; Weber and Penn, 1995). Classical modular representations have

120 been completed based on systems of branch, axis and different types of growth units or

121 internodes. In addition to this, a statistical approach, illustrated by Guédon *et al*. (2001),

122 has become essential for the analysis of architectural data. The statistical framework of

123 the hidden Markov tree (HMT) model was introduced by Crouse *et al*. (1998) for

124 modelling a tree-structured process. Markovian models for tree-structured data have

125 been integrated into the AMAPmod software (Godin *et al*., 1997).

126

127 Therefore, there are to date several methods for generating virtual trees and in particular

128 fruit trees. On the other hand, recent research has demonstrated the benefits of LS as

129 crop sensors and their application in different areas. However, doubts arise when

130 considering how to use these devices in field conditions or, as it is called, in a real

131 LiDAR system operation (LSO). In this regard, many field tests would be unnecessary

132 if simulators of LiDAR operation in virtual orchards could be available. Assuming

133 virtual trees are close to reality, LiDAR system simulators (LSS) can be used to

134 optimise the configuration of LSO for the estimation of canopy volumes and tree foliage

135 surfaces for different precision agricultural practices as plant protection, fertilisation and

136 precise irrigation (Garrido *et al*., 2012). Other possible application could be the

137 simulation of light distribution within the canopies given its influence on crop growth

138 and yield. Estimation of shaded area by the canopy is also gaining relevance due to its

139 relation with precision irrigation scheduling and water demand of crops. Finally,

140 evaluating virtual trees (or tree models) can be performed using the LSS as validation.

141 In fact, the LSS would allow testing of the sensibility of parameters obtained in a real

142 LSO survey by performing different virtual processes in creating trees. As suggested by

143 Delagrange and Rochon (2011), the idea being to verify which growth-pattern allows a

144 virtual tree close to the original tree. Once validated, the virtual tree can substitute the

145 need of manual defoliation to measure the leaf area index (LAI), among other

146 parameters.

147

148 To sum up, LSS programs would allow the processes of growth and vegetative

149 characteristics for virtual trees to be investigated. In this regard, the aim of this study is

150 to develop simulation software to obtain fruit trees and the subsequent operation of a

151 virtual LiDAR sensor or LSS. The trees should be able to include both ligneous and

152 orchard's foliar structure. The subsequent validation consists in comparing the

153 simulated characteristics of trees with the parameters obtained with the LSS. Ultimately,

154 it is intended that researchers and users of LS will have a useful tool for configuring

155 terrestrial laser sensors in real operations (LSO).

156

157 2. *MATERIALS AND METHODS*

158 The software presented here is an application developed in C++ that improves an early

159 version (SIMLiDAR, Méndez *et al*., 2012). Firstly, the user can generate a virtual

160 orchard (or canopy geometry) using a Lindenmayer, L-system, (Tarquis and González-

161 Andrés, 1995; Tarquis *et al*, 2006), or a Hidden Markov Tree modelling process, HMT

162 (Durand *et al*., 2005; Costes *et al*., 2008). The generated tree depends on different plant

163 parameters (number of reiterations, transition probabilities, phyllotaxis angle), being

164 possible with this new version providing an own site with a three-dimensional scene

165 based on OpenGL™ (http://www.opengl.org).

166

167 After obtaining the virtual tree, the program allows the simulation of a terrestrial laser

168 scanner (LSS), and then determining some vegetative parameters from this simulation.

169 Concerning data from the LSS, the program provides a set with the distances from laser

170 beam origin to nearby plant objects (branches or leaves). The current work is focused on

171 the estimation of actual foliar surface from parameters obtained using beam impacts. A

172 method that correlates several impacted areas in a real laser operation (LSO) and leaf

173 area (virtual orchard) was considered.

174

2.1. An improved hidden Markov tree (HMT) model for artificial

175

orchards

176

177 The plant architecture starts from the foliar development of the apical meristem (Bell

178 1994) that can undergo an undefined (monopodial) or defined (sympodial) growth. The

179 model of vegetative development stems from the combination of different types of axis

180 with morphological characteristics as growth patterns, branching type, phyllotaxis or

181 spatial orientation. The architectural unit of the plant depends on the type of axis and

182 growth model used. Growth occurs with axis production already present in previous

183 stages, known as the reiteration process. Reiteration is a mechanism that allows building

184 of the crown in the majority of trees (Barthélémy *et al.*, 1991). Analysis of the plant

185 architecture enables a detailed quantitative analysis (Tourn *et al.*, 1999) that allows

186 measurement of the growth in structural units (Godin *et al.*, 1997; Blaise *et al.*, 1998).

187 These models describe the meristem development from stochastic processes (De Reffye

188 *et al.*, 1991). On the other hand, it is possible to extract a distribution of axes in different

189 kinds of metamer sequences or growth unit (GU) from quantitative studies. The

190 metamer sequence is assimilable to a set of mutually exclusive random states. Crouse *et*

191 *al.* (1998) introduced a hidden Markov tree (HMT) to model homogeneous areas. The

192 number of states is determined using stochastic criteria. Detailed studies of apple trees

193 have been carried out over branching patterns in 1-year trunks (Costes & Guédon,

194 2002), and in the architectural development of 6-year old trees (Costes *et al.*, 2003)

195   applying the HMT to plant architecture (Durand *et al.*, 2004) and with a stochastic and

196   biomechanical model (Costes *et al.*, 2008).

197

198   In this work, the development of a virtual tree is based on a structure of axes that, by

199   reiteration, is expanded with new metamers that transit into different states. The

200   transition from one state to the next is regulated according to a stochastic process based

201   on a probability matrix belonging to a first order Markov chain. Specifically, the

202   stochastic summary presented by Durand *et al.* (2005) in a transition matrix of four

203   states is used (Table 1). The states defined by Durand correspond to the macroscopic

204   states used in the software MappleT (Costes *et al.*, 2008). These four states are long,

205   medium, short and floral (L, M, S, F). Each state contains an average number of

206   metamers (20, 8, 1 and 3, respectively). Adjustments have been introduced to determine

207   the number of metamers according to the order number and age of the axes (Costes *et*

208   *al.*, 2003). The results of the functions $Ni = 96.436 \, e^{-0.37 \cdot Ta}$ for trunks, and

209    $Ni = 68.525 \, e^{-0.33 \cdot Ta}$ for long shoots are tabulated in Table 2, where *Ta* is the tree age

210   and *Ni* the number of internodes. The model adopted is developed with the following

211   entities: axis, branch and leaf. The branches and leaves depend on the state (transition

212   matrix) of the axes. In fact, a branch corresponds in our model to a growth unit (GU)

213   that could be different depending on the axis state. In a particular transition, the

214   previous and following states are evaluated to determine the existence of apical

215   succession or sympodial branching. Apical succession only involves the creation of a

216   shoot according to the new state of the axis. Each shoot is a succession of metamers

217   (one internode and one leaf), with the number of metamers shown in Table 2 and leaves

218   following phyllotaxis rules. However, if there is a sympodial branching, a new axis is

219   created using a fixed branching angle (to 35º) over the current axis direction. Up to

220   three new axes can be created if the new state accepts all internodes. If the new state is

221   developed from a short state (S, single internode), only one axis is created in the

222   branching process.

223

224   The tree is initiated with a long first state (L), which determines the initial probability of

225   the Markov chain. So, the (L, M, S, F) probability vector is (1,0,0,0). To make possible

226   both growth options (apical succession or sympodial branching), the model uses two

227   basic morphological functions that control the plant growth, the succession (noted as >)

228   and the branching (noted as +). Durand *et al*. (2005) propose the use of two probability

229   matrices to control both processes separately, although it is usual to use rules to control

230   succession (>) and branching (+) depending on previous and following states (Costes *et*

231   *al*., 2003, Durand *et al*., 2005; Costes *et al*., 2008). Moreover, straight axes are used

232   because biomechanical correction to introduce tropism effects has not been considered

233   (as is done by Costes *et al*., 2008). During a transition every axis is evaluated. To do

234   this, the axis probability P^k is considered, P being the probability matrix proposed in

235   Table 1 and k the number of transitions occurred in this axis. For instance, if a u vertex

236   is in S_u state, the transition probability will be defined by a matrix $P = \left(p_{ij} \right)$, where

237    $p_{ij} = P(S_u = j | S_\rho(u) = i)$ represents the probability of a change from the i -th state in

238   the $\rho(u)$ parent vertex to the state j in the u vertex (Fig. 1).

239

240   Each stage is formalised mathematically as follows. Given a unitary direction **d** from a

241   point O, it is possible to obtain a new direction **d'** that has an α angle with the above

242   mentioned rotation around point O. To do this, an intermediate normal direction **n** to a

243   plane that contains the fixed point O and the direction **d** is required. Figure 2 shows the

244   procedure used to achieve this rotation. Specifically, the normal vector **n** is obtained by

245   the vector product $\mathbf{n} = \mathbf{d} \times \mathbf{d_2}$, in which $\mathbf{d}_2$ is a direction not aligned to $\mathbf{d}$ and established

246   arbitrarily. The application of Eq. 1 allows obtaining finally the new growth direction.

247

248     $$\mathbf{d}' = \cos\alpha\,\mathbf{d} + \sin\alpha\,(\mathbf{n} \times \mathbf{d}) + (1 - \cos\alpha)(\mathbf{n} \cdot \mathbf{d})\,\mathbf{n} \tag{1}$$

249

250   The arbitrary selection of $\mathbf{d}_2$ only has influence on the initial phyllotaxis angle which is

251   applied to the first new branch in a current axis. Since there is no preference for the

252   direction of growth, the consecutive branches are turned $\mathbf{d}'$ from $\mathbf{d}$ (Fig. 2d) following a

253   fixed phyllotaxis angle (set to 144º in the current work according to Costes *et al*., 2008).

254   Thus, Eq. (1) changes to Eq. (2) using $\mathbf{d}$ instead of $\mathbf{n}$, **d'** instead of **d**, and α taking

255   values with phyllotaxis angle increments.

256

257     $$\mathbf{d}'' = \cos\alpha\,\mathbf{d}' + \sin\alpha\,(\mathbf{d} \times \mathbf{d}') + (1 - \cos\alpha)(\mathbf{d} \cdot \mathbf{d}')\,\mathbf{d}$$

258     $$\tag{2}$$

259   From experimental measurements of fruit tree canopies it was observed that the foliar

260   distribution is greater in the outlying space, tending to maximise the solar exposure

261   (Sanz *et al*., 2011). However, the foliar distribution within the canopy in the virtual

262   model becomes thicker as the number of reiterations increases. To reduce this effect, an

263   algorithm that evaluates the shady index for each leaf is proposed. Thus, if the shady

264   ratio reaches a threshold (model parameter), the leaf is removed in the process of

265   generating the virtual tree. Marking the center of gravity of each leaf, the algorithm uses

266   several semi-straights from this point to the infinity to search for any impact with other

267   leaves. To get an acceptable processing time for this algorithm, the number of semi-

268   straights must be necessarily limited. The semi-straights are selected according to a

269   semi-spherical distribution in two directions β (polar angle) and φ (azimuth angle).

270   The polar angle ranging between $[0^{o}, 360^{o}]$ and angular increments $\Delta\beta = 45^{o}$ were

271   used. In the case of the azimuth angle values were $[-90^{o}, 90^{o}]$ and $\Delta\varphi = 15^{o}$,

272   respectively. The proposed method is independent of the shape of the tree canopy and

273   does not require any type of data structure to support the calculation. Finally, the leaf

274   area L_A for the virtual tree is measured as the sum of the individual areas of all the

275   leaves of the orchard.

276

277   Figure 3 (a) shows an example of the HMT apple tree model. To obtain this virtual

278   orchard several parameters were used. Some parameters were previously fixed; the user

279   can vary several others. However, the options considered were as follows.

280

281   • The dimension of the Markov model was set equal to 4. The probability matrix

282   dimension and the number of different states depend on this parameter.

283   • The character strings that represent each state were L, M, S and F (Long,

284   Medium, Short and Floral, respectively).

285   • The program operated on two probability matrices (one for succession and

286   another for branching). Both were set to the same values according to Table 1.

287   • The branching angle was 35º.

288   • The phyllotaxis angle was 144º.

289   • The program allows the maximum number of new branches that can be obtained

290   from the parent GU in the branching process to be set.

291   • Initial GU and initial direction were set to L state and (1,0,0) vector direction.

292   Both define the first axis of the plant before starting the reiteration process.

293   • The internode length was 35 mm.

294   • The number of internodes used by state, axis order and birth year were set

295   according to the values in Table 2.

296   • Branching and succession rules were established by parent-child state according

297   to Table 3.

298

299   ***2.1.1. Other kinds of models***

300   The new model presented in this paper continues to support the L-System model

301   developed by Méndez *et al*. (2012). Thus, it is also possible to upload a virtual tree

302   generated by an external tool provided that there is an interface for branches and leaves

303   based on text files. For the branches, it is necessary to know the (*x, y, z*) coordinates

304   from both the ends of the branch and the value of the diameter. For the leaves, (*x, y, z*)

305   coordinates of the leaf external polygonal chain or polyline must be known.

306

307   A Lindenmayer system (L-system) (Lindenmayer, 1968) builds complex objects, as a

308   branching pattern of a tree, by successively replacing parts of an initial object using a

309   set of rewriting rules or productions (R). The rewriting rules, proposed by Von Koch

310   (1905) operate on character strings, or alphabet (Ω), as a formal grammar (Chomsky,

311   1956). The rewriting process starts from a distinguished string, called the axiom (w) that

312   represents a budding tree. In each iterative step the active bud is replaced by a new

313   branch structure so, for example, active buds and branches are letters of the alphabet.

314   Prusinkiewicz and Lindenmayer (1990) define a deterministic L-system as a triplet {Ω,

315   w, R}, where Ω is the alphabet, w the axiom and R the productions set. The process has

316   two stages; in the first a string substitution is carried out from the initial string (w)

317   replacing a letter by a new substring according to production rules (R). Every symbol is

318   replaced in the string as many times as it appears. At the end of the first stage a final

319   string is obtained, which is interpreted according to turtle geometry (Abelson & diSessa,

320   1982). A turtle is an intrinsic geometry that can be assimilated to a drawing cursor in

321   3D, with two parameters (position and orientation) that describe the virtual plant

322   modelling.

323

324   *2.2. Simulation of the laser sensor*

325   The virtual tractor-mounted LiDAR advances along the row (OY axis), and the laser

326   beam is directed towards the interior of the vegetation (OX axis). Through a secondary

327   angular movement in the XZ plane the scanner measures the distances to the virtual

328   orchard, as shown in Méndez *et al.* (2012) for ligneous models. In the current work,

329   leaves are included in the model resolving the scan simulation with two basic

330   movements. The main movement (y) is a cross-sectional advance along the OY axis

331   from a starting point y_1, carrying out successive incremental advances of Δy (simulation

332   parameter). A secondary angular movement (θ) takes place between two fixed angular

333   values (θ_{min} and θ_{max}) at a given position of the OY axis (y_i). Thus, the laser beam

334   advances incrementally by $\Delta\theta$, which is also a parameter in the program. In each

335   displacement of y_i, angles θ_{min} and θ_{max} are calculated from the laser sensor position

336   and the maximum plant height. Finally, at each position of the laser beam (y_i, θ_k), a

337   search is performed for the impacts between the virtual laser beam and the leaves of the

338   modelled tree.

339

340   The set of impacts between leaves and laser beams is found by solving a straight

341   line/plane intersection problem because the leaves are modelled by plane closed

342   polygons. The branches/laser beam intersection is quite different. The end of the laser

343   beam is modelled as a small three-dimensional mesh and an intersection is considered

344   when some point of the mesh is inner to the branch trunk cylinder (Méndez *et al.*,

345   2012). If the laser beam is not intercepted by the tree, it may be intercepted by the

346   ground (when $\theta < 0$) or, in some cases, it may not be intercepted at all (when $\theta > 0$). In

347   the first case the distance to the ground is recorded, while in the second case an escape

348   distance is recorded (in fact, a constant is used with a distance much greater than any

349   possible interception). The result of the simulation is a matrix L where each $l_{i,k}$ element

350   is the laser beam distance from LiDAR to the tree model in each (y_i, θ_k) laser position.

351   In matrix L i = 1, …, N is the number of different laser beams depending on the

352   resolution used, and k = 1, …, M, is the number of increments (Δy) along the tractor

353   route.

354

355   The LiDAR simulation (LSS) is done through lateral measurements from one side of the

356   tree. The lateral operation of LiDAR from the opposite side is also included in the

357   simulation. It could be established an internal coordinated reference that links both

358   processes, because each row is related with a *y* value of cross-section advance. In any

359   case, it is sufficient to simulate only one side of the vegetation for estimating the leaf

360   area and other vegetative parameters. Moreover, a third option may be used in the

361   simulation of the scanning process. Specifically, a new zenith position of LiDAR is

362   included, assuming that the scanning is carried out overhead at a sufficient height

363   (simulating an aerial scan). Besides all this, the program can perform angular (default)

364   and also orthogonal scanning. The latter could only be applied when the distance of the

365   laser to tree is very large (for example, overhead), or to simulate several lasers mounted

366   in a vertical bar. In this case, the laser beams are projected parallel to the OX axis, so

367   the system records the distances from the LiDAR to the parallel YZ planes resulting

368   from different intercepts (Fig. 4). The program also permits virtual scanning on two

369   rows, getting different random trees in both. In such cases a specific simulation operates

370   by moving the tractor in the middle of the two rows. The result is two files for the scan

371   of each side, left or right.

372

373   To detect the impacts, a scanner position $\mathbf{P} = \begin{pmatrix} x & y & z \end{pmatrix}$ is assumed (Fig. 5). When an

374   impact occurs, the intercept point ($\mathbf{R}$) must belong to the straight line

375   $\mathbf{R} = \mathbf{P} + t \cdot \mathbf{d}$ $(t \in \Re)$, with $\mathbf{d}$ being the unitary direction of the laser beam. When the

376   polyline of a leaf containing the point Q and following an orthogonal direction w

377   impacts with the laser beam occurs, the expression $t = \pm \dfrac{(\mathbf{P} - \mathbf{Q}) \cdot \mathbf{w}}{\mathbf{d} \cdot \mathbf{w}}$ will be true, with

378   $\mathbf{R}$ being an inner point of the leaf (Fig. 5). The values of $\mathbf{P}$ and $\mathbf{d}$ will depend on the

379   type of scan selected in Table 4. The interception between the laser beam and the

380   ligneous structure is solved according to the criteria of Méndez *et al.* (2012). Thus, the

381   interception between the laser beam and a branch is calculated using a dot matrix. A set

382   of points are evaluated to determine if they are inner to a cylindrical trunk object, and

383   then it is decided whether the laser beam does or does not intercept a branch.

384

385   *2.2.1. Leaf area and tree measurements*

386   A standard LiDAR operation gets a matrix of the distances measured. Every distance is

387   related with an angular position of the laser beam and an average angular and cross-

388   advance increase can be considered for all the operation. All previous data allow a

389   discrete impacted area for each laser beam to be estimated, being the sum of all the

390   impacted total area (I_T) of a LiDAR operation. The program could measure I_T in this

391   manner. However, as the program has established which objects are branches or leaves,

392   it can also differentiate which impacts occur at a leaf object and sums them, thus

393   obtaining the impacted leaf area (I_L). Moreover, when the program finds an impact with

394   a leaf, it extends the direction of the laser beam to count secondary intersections with

395   other leaves behind the first one. It sums these discrete areas into the so-called impacted

396   area in the three outer layers of leaves (I_{3L}). The extension of the laser beam direction

397   founding secondary leaves stops if a branch object is found. In the virtual model the

398   leaves and wood objects are typified to distinguish easily where the impact has

399   occurred. This does not happen in a real LiDAR operation. Since the virtual leaf area

400   (L_A) is known, a regression analysis may be performed to predict L_A using the

401   parameters of LiDAR simulation (I_T, I_L and I_{3L}). In any case, the regression analysis is

402   used as LiDAR validation procedure.

403

404   ***2.2.2. Formulas used in the model***

405   When a laser beam hits a branch or leaf, the impacted total area is considered to be the

406   projection on the YZ plane obtained by the following equation:

407

408   $$\Delta y \cdot \left[\left(z_0 + l_{ij} \cdot \sin\left(\theta_j + \Delta\theta\right)\right) - \left(z_0 + l_{ij} \cdot \sin\theta_j\right)\right] \tag{3}$$

409

410   where z_0 is the height of the laser above the ground, and l_{ij} and θ_j are the distance and

411   the impact angle, respectively. As such, the total detected (impacted) area will be equal

412   to

413

414   $$I_T = \sum_{i,j} \Delta y \cdot \left[\left(z_0 + l_{ij} \cdot \sin\left(\theta_j + \Delta\theta\right)\right) - \left(z_0 + l_{ij} \cdot \sin\theta_j\right)\right] \tag{4}$$

415

416   The impacted leaf area (I_L) is obtained considering only the impacts on leaves and also

417   using Eqs. (3) and (4). However, the impacted area in the three outer leaves (I_{3L}) is

418   different as it is obtained by applying Eqs. (3) and (4) up to a maximum of the first three

419   leaves (or layers) in the tree, provided that no woody structure is intercepted before

420   (Fig. 6). Therefore, it is expected that intuitively the magnitude of the three impacted

421   areas may be ordered as $I_L < I_T < I_{3L}$. These areas are then used as regressor variables

422   to predict the leaf area (L_A) of simulated apple trees.

423

424   ### 2.3. Tests to evaluate the simulation program

425   Twenty different virtual orchards were obtained by the HMT model. The number of

426   iterations in the process and the shady index were varied to obtain apple trees with

427   different structure and geometry. Specifically, orchards were obtained after applying 7,

428   8, 9, 10 or 11 iterations. The shady percentages were 60, 70, 80 and 101 (the latter

429   indicated that no shading was considered and no leaves were removed at the end of the

430   simulation process). Concerning the LiDAR simulation, two scanning processes were

431   performed, according to the sensor position and the laser beam projection. First, the

432   sensor was simulated in lateral position and projecting the beam angularly with respect

433   to the row. In the other case, the sensor was simulated in zenith position and orthogonal

434   projection of the beam. In terms of formulas, the horizontal resolution (or cross-

435   sectional increment) was set to $\Delta y = 0.002$ m. An angular resolution of $\Delta\theta = 0.25^\circ$ was

436   used when the beam was simulated with angular projection.

437

438   ### 3. RESULTS AND DISCUSSION

439   The LiDAR sensor simulation developed here reported some interesting results. As

440   intended, the LSS has allowed to evaluate the performance of a LiDAR sensor in real

441   operating conditions (LSO) using in this case virtual apple trees. The first consideration

442   to note is that the sensor may have different behaviour depending on the mode of use.

443   There was a very satisfactory estimate of tree leaf area (L_A) when the LiDAR sensor was

444   used from the side of the row (which is the normal position of use). However, the use of

445   the sensor from an elevated position, above the row, slightly improved the previous

446   results. The reasons for this effect are unclear. However, some discussion could be

447   made on the basis of the regression models obtained. Overall, a good linear correlation

448   was found between the aforementioned leaf area of virtual trees (L_A) and the impacted

449   areas using the LiDAR (I_L, I_T, and I_{3L}) (Fig. 7).

450

451   For the lateral scanning process Eqs. (5), (6) and (7) show different behaviour near the

452   origin. In fact, only the model that computed all impacts (i.e. leaves and wood)

453   presented an intercept. This was an expected result, since with leafless trees the

454   impacted area will always be greater than zero due to the presence of branches. This

455   effect also occurs in the zenith scan.

456

457    $$L_A = 12.67 \cdot I_L \ \left(R^2 = 0.95\right)$$ (5)

458    $$L_A = 8.70 \cdot I_T - 209.15 \ \left(R^2 = 0.94\right)$$ (6)

459    $$L_A = 6.40 \cdot I_{3L} \ \left(R^2 = 0.97\right)$$ (7)

460

461   Another interesting effect is the value of the regression coefficients. Given that

462   impacted leaf area (I_L) was lower than impacted total area (I_T), the regression analysis

463   gave a higher regression coefficient (12.67) for the regressor variable I_L in comparison

464   with I_T (8.70). The lowest regression coefficient (6.40) corresponded to the variable I_{3L}

465   which was expected since the surface impacted in the first three leaves is greater than in

466   others. The same trend has occurred when the sensor scanned from overhead. Equations

467   (8), (9) and (10) were obtained for this case.

468

469    $$L_A = 7.10 \cdot I_L \ \left(R^2 = 0.97\right) \tag{8}$$

470    $$L_A = 6.71 \cdot I_T - 129.84 \ \left(R^2 = 0.96\right) \tag{9}$$

471    $$L_A = 3.29 \cdot I_{3L} \ \left(R^2 = 0.99\right) \tag{10}$$

472

473   Comparing both procedures it was noted that zenith scans always provided regression

474   coefficients lower than the corresponding lateral equations. This may be due to the

475   growth pattern and training system of the simulated tree structure. Using LiDAR

476   measurements Sanz *et al*. (2011) have shown that trees tend to grow laterally by

477   opening the canopy for a better use of sunlight. More specifically, leaves tend to grow

478   outward from the canopy for light for photosynthesis. This probably causes an increased

479   foliar exposure from an overhead view as opposed to a lateral one, which is more

480   obvious when the open vase form was adopted as the growth pattern (or training

481   system) in the HMT modeling. Therefore, it is not surprising that using the LiDAR

482   sensor overhead increased the number of impacts of the laser beam. Thus, the impacted

483   areas were larger making the results of regression analysis more consistent. The

484   question now is how to take advantage of this type of simulation; before or after using a

485   LiDAR sensor operating in the field (LSO).

486

487   Before using the sensor in field conditions, the LSS can be used to test and optimise the

488   main parameters of a real LiDAR operation. Among the basic parameters are the

489 horizontal (Δy) and the angular ($\Delta\theta$) resolution of the scanning process. The data to be

490 processed depends on these parameters, and it is advisable to reduce the acquired

491 information while ensuring the accuracy of the measurement. To test the effect of

492 scanning resolution on the impacted total area (I_T), a sensitivity analysis was carried out.

493 Table 5 shows the error that occurs when the horizontal distance between scans (Δy)

494 increases relative to an increment of 2 mm taken as reference. The usefulness of this

495 analysis is clear. Assuming a maximum error of 5%, the LiDAR sensor could be used

496 by separating each scan by a distance of 20 mm.

497

498 Concerning the post-processing of a real operation with LiDAR sensor, secondary

499 measures can be estimated using the predetermined regressions with the LSS. From data

500 obtained from a LiDAR operation the impacted total area (I_T) can be calculated. Then,

501 Eq. (6) can be applied to estimate L_A if the LSO has been carried out by moving

502 laterally. Subsequent estimation of leaf area index (LAI) is immediate if the distance

503 between rows is also known. However, since the LSS has knowledge of the error

504 associated with the scan resolution, overestimation of I_T can be corrected for by

505 providing a more realistic value of L_A through the corresponding regression equation.

506

507 In short, the LSS developed in this work appears to be a reliable tool for predicting the

508 leaf surface area of fruit trees. Furthermore, the LSS is easy to use. The program runs on

509 a Windows operating system, and can be installed on a personal computer with a

510 standard processor and reasonable memory capacity. The user can take advantage of

511 this utility through subsequently developing new libraries to scan real orchards. For the

512 moment, a snapshot of an orchard model is obtained and can be used as many times as

513 necessary. This is especially interesting for ensuring repeatability and separate sensor-

514 environment interaction.

515

516 ## *4. CONCLUSIONS*

517 A simulation program applied to fruit trees which generates an artificial orchard using a

518 Hidden Markov Tree (HMT) model has been developed. The program simulates the

519 growth pattern of an apple tree grown with open vase training system. Once a virtual

520 tree is obtained, the user can simulate and predict the performance of a LiDAR system.

521 The areas resulting from laser sensor impacts are then used to predict the tree leaf

522 surface. The virtual tree derived by the HMT model was improved by introducing a

523 shady index to approximate the distribution of the leaves to the experimental

524 observations of actual tree canopies. Furthermore, this foliar correction can be applied

525 to any training system since it does not depends on the shape of the tree. As for the

526 LiDAR system simulator (LSS), the user can choose between a lateral scanning process

527 or, instead, an overhead scanning process. Both procedures showed good prediction of

528 the leaf area (L_A) from the impacted area (I_T). Derived from this, the program should

529 have applications in two main fields. Firstly, the LSS is useful for laser calibration of a

530 real LiDAR system operation (LSO). The user can compare different scanning

531 resolutions in different scenarios allowing them to decide which the best system

532 configuration is. The advantage in reduced time, equipment and precision is evident.

533 Secondly, LSS is also very useful in post-processing. Data acquired in real operating

534 conditions (LSO) can be converted to vegetative measurements using suitable

535 regression formulae. Vegetative data that cannot be measured in a LSO could be

536 obtained through the LSS regressions. Thus, both end users and researchers can take

537 advantage of the optimal configuration of LiDAR systems and better characterisation of

538 scanned fruit trees.

539

540 ***REFERENCES***

541

542 Abelson, H. & di Sessa, A. Turtle Geometry. (1982). M.I.T. Press, Cambridge.

543 Arnó, J., Escolà, A., Vallès, J.M., Llorens, J., Sanz, R., Masip, J., et al. (In press). Leaf

544   area index estimation in vineyards using a ground-based LiDAR scanner.

545   Precision Agriculture. DOI: 10.1007/s11119-012-9295-0.

546 Barthélémy, D., Edelin, C. & Halle, F. (1991). Canopy Architecture. In: Physiology of

547   trees (ed A.S. Raghavendra), pp. 1-19. J. Willey & Sons, Inc. London.

548 Bell, A. (1994). A summary of branching process in plants. In: Shape and form in plants

549   and fungi (eds. D.S. Ingram & A. Hudson), pp. 119-142. Academic Press,

550   London.

551 Blaise, F., Barczi, J.F., Jaeger, M., Dinouard, P. & de Reffye, P. (1998). Simulation of

552   the growth of plants. Modelling of metamorphosis and spatial interactions in

553   architecture and development of plants. In: Cyberworlds (eds. T.L. Kunii & A.

554   Luciani), pp. 81-109. John Wiley & Sons, Tokyo.

555 Chomsky, N. (1956). Three models for the description of language. IRE Trans. on

556   Information Theory, 2(3):113–124.

557 Costes, E. & Guédon, Y. (2002). Modelling branching patterns on 1-year-old trunks of

558   six apple cultivars. *Annals of Botany,* 89: 513–524.

559 Costes, E., Sinoquet, H., Kelner, J.J. & Godin, C. (2003). Exploring within-tree

560   architectural development of two apple tree cultivars over 6 years. *Annals of*

561   *Botany,* 91: 91-104.

562   Costes, E., Smith, C., Renton, M., Guédon, Y., Prusinkiewicz, P. & Godin, C. (2008).

563   MAppleT: simulation of apple tree development using mixed stochastic and

564   biomechanical models. *Functional Plant Biology*, 35: 936–950.

565   Crouse, M.S., Nowak, R.D. & Baraniuk, R.G. (1998). Wavelet-based signal processing

566   using hidden Markov models. *IEEE Transactions on Signal Processing*, 46: 886–

567   902.

568   Dauzat, J. (1993). Simulated plants and radiative transfer simulations, in: Varlet-

569   Grancher C., Bonhomme R., Sinoquet H. (Eds.), Colloque Structure du Couvert

570   Végétal et Climat Lumineux: méthodes de caractérisation et applications, INRA

571   Editions, Saumane, France, pp. 271-278.

572   Dauzat, J., Rapidel, B. & Berger, A. (1999). Simulation of leaf transpiration and sap

573   flow in virtual plants: description of the model and application to a coffee

574   plantation in Costa Rica, *Agricultural and Forest Meteorology*, 109(2): 143-160.

575   Delagrange, S. & Rochon, P. (2011). Reconstruction and analysis of a deciduous

576   sapling using digital photographs or terrestrial-LiDAR technology. *Annals of*

577   *Botany,* 108: 991–1000.

578   De Reffye, P., Elguero, E. & Costes, E. (1991). Growth units construction in trees: a

579   stochastic approach. *Acta Biotheoretica*, 39: 325-342.

580   De Reffye, P., Fourcaud, T., Blaise, F., Barthélémy, D. & Houllier, F. (1997). A

581   functional model of tree growth and tree architecture. *Silva Fenn.,* 31(3): 297-311.

582   Diggle, A.J. (1988). ROOTMAP-A model in three-dimensional coordinates of the

583   growth and structure of fibrous root systems. *Plant Soil*, 105: 169-178.

584   Durand, J.B., Gonçalvès, P. & Guédon, Y. (2004). Computational methods for hidden

585   Markov trees – an application to wavelet trees. *IEEE Transactions on Signal*

586   *Processing*, 52: 2551–2560.

587   Durand, J.B., Guédon, Y., Caraglio, Y. & Costes, E. (2005). Analysis of the plant
588   architecture via tree-structured statistical models: the hidden Markov tree models.
589   *New Phytologist*, 166: 813–825.

590   Ehlert, D., Heisig, M. & Adamek, R. (2010). Suitability of a laser rangefinder to
591   characterize winter wheat. Precision Agriculture, 11(6): 650-663.

592   Escolà, A., Camp, F., Solanelles, F., Llorens, J., Planas, S., Rosell, J.R., et al. (2007).
593   Variable dose rate sprayer prototype for tree crops based on sensor measured
594   canopy characteristics. In: Precision Agriculture '07. Proceedings of the 6th
595   European Conference on Precision Agriculture, Skiathos, Greece, 3-6 January
596   2007.

597   Fisher, J.B. & Weeks, C.L. (1985). Tree architecture of Neea Nyctaginaceae: geometry
598   and simulation of branches and the presence of two different models.,. 7, 385-401.

599   Früh, T. (1997). Simulation of water flow in the branched tree architecture. *Silva*
600   *Fennica*, 31(3): 275-284.

601   Ford, E.D., Avery, A. & Ford, R. (1990). Simulation of branch growth in the Pinaceae:
602   interactions of morphology, phenology, foliage productivity, and the requirement
603   for structural support, on the export of carbon. *J. Theor. Biol.*, 146: 15-36.

604   Garrido, M., Méndez, V., Valero, C., Correa, C., Torre, A. & Barreiro, P. (2012).
605   Online dose optimization applied on tree mass through a laser device. First RHEA
606   International Conference on Robotics and associated High-technologies and
607   Equipment for Agriculture. University of Pisa, September 19-21, 2012.

608   Gebbers, R., Ehlert, D. & Adamek, R. (2011). Rapid mapping of the leaf area index in
609   agricultural crops. Agronomy Journal, 103(5): 1532-1541.

610 Gil, E., Escolà, A., Rosell, J.R., Planas, S. & Val, L. (2007). Variable rate application of

611   plant protection products in vineyard using ultrasonic sensors. *Crop Protection* ,

612   26(8): 1287-1297.

613 Guédon, Y., Barthélémy, D., Caraglio, Y. & Costes, E. (2001). Pattern analysis in

614   branching and axillary flowering sequences. *Journal of Theoretical Biology*, 212:

615   481–520.

616 Godin, C., Guédon, Y., Costes, E. & Caraglio, Y. (1997). Measuring and analyzing

617   plants with AMAPmod software. In: Plants to ecosystems. (ed. M.T.

618   Michalewicz.), pp. 53-84. CSIRO, Australia.

619 Harper, J.L., Rosen, B.R. & White, J. (1986). The growth and form of modular

620   organisms, The Royal Society, London, UK.

621 Holmgren, J., & Persson, A. (2004). Identifying species of individual trees using

622   airborne laser scanner. *Remote Sensing of Environment*, 90(4): 415-423.

623 Llorens, J., Gil, E., Llop, J. & Escolà, A. (2011). Ultrasonic and LiDAR Sensors for

624   Electronic Canopy Characterization in Vineyards: Advances to Improve Pesticide

625   Application Methods. *Sensors*, 11(2): 2177-2194; doi: 10.3390/s110202177.

626 Lefsky, M.A., Cohen, W.B., Acker, S.A., Parker, G.G., Spies, T.A. & Harding, D.

627   (1999). Lidar Remote Sensing of the Canopy Structure and Biophysical Properties

628   of Douglas-Fir Western Hemlock Forests. *Remote Sensing of Environment*, 70(3):

629   339-361.

630 Lindenmayer, A. (1968). Mathematical models for cellular interaction in development,

631   Parts I and II. *Journal of Theoretical Biology*, 18: 280-315.

632 Maltamo, M., Eerikäinen, K., Pitkänen, J., Hyyppä, J. & Vehmas, M. (2004).

633   Estimation of timber volume and stem density based on scanning laser altimetry

634   and expected tree size distribution functions. *Remote Sensing of Environment,*

635   90(3): 319-330.

636 Méndez, V., Catalán, H., Rosell, J.R., Arnó, J., Sanz, R. & Tarquis, A. (2012).

637   SIMLiDAR – Simulation of LiDAR performance in artificially simulated

638   orchards. *Biosystems Engineering,* 111(1): 72-82.

639 Omasa, K., Hosoi, F. & Konishi, A. (2007). 3D lidar imaging for detecting and

640   understanding plant responses and canopy structure. *Journal of Experimental*

641   *Botany,* 58(4): 881-898.

642 Palacín, J., Pallejà, T., Tresánchez, M., Sanz, R., Llorens, J., Ribes-Dasi, M., et al.

643   (2007). Real-time tree-foliage surface estimation using a ground laser scanner.

644   *IEEE Transactions on Instrumentation and Measurement,* 56(4): 1377-1383.

645 Parker, G., Harding, J. & Berger, M. (2004). A portable LiDAR system for rapid

646   determination of forest canopy structure. *Journal of Applied Ecology,* 41(4): 755-

647   767.

648 Prusinkiewicz, P. & Lindenmayer, A. (1990). The algorithmic beauty of plants,

649   Springer Verlag, New York.

650 Riaño, D., Chuvieco, E., Condés, S., González-Matesanz, J. & Ustin, S.L. (2004).

651   Generation of crown bulk density for Pinus sylvestris L. from lidar. *Remote*

652   *Sensing of Environment,* 92(3): 345-352.

653 Rosell, J.R., Llorens, J., Sanz, R., Arnó, J., Ribes-Dasi, M., Masip, J., et al. (2009a).

654   Obtaining the three-dimensional structure of tree orchards from remote 2D

655   terrestrial LiDAR scanning. *Agricultural and Forest Meteorology,* 149(9): 1505-

656   1515.

657 Rosell, J.R., Sanz, R., Llorens, J., Arnó, J., Escolà, A., Ribes-Dasi, M., et al. (2009b). A

658   tractor mounted scanning LiDAR for the nondestructive measurement of

659 vegetative volume and surface area of tree-row plantations: a comparison with

660 conventional destructive measurements. *Biosystems Engineering*, 102(2): 128-

661 134.

662 Rosell, J.R. & Sanz, R. (2012). A review of methods and applications of the geometric

663 characterization of tree crops in agricultural activities. *Computers and Electronics*

664 *in Agriculture,* 81: 124-141. DOI:10.1016/j.compag.2011.09.007.

665 Saeys, W., Lenaerts, B., Craessaerts, G. & De Baerdemaeker, J. (2009). Estimation of

666 the crop density of small grains using LiDAR sensors. *Biosystems Engineering,*

667 102(1): 22-30.

668 Sanz, R., Llorens, J., Escolà, A., Arnó, J., Ribes-Dasi, M., Masip, J., et al. (2011).

669 Innovative LiDAR 3D dynamic measurement system to estimate fruit-tree leaf

670 area. *Sensors,* 11: 5769-5791.

671 Scala, J.J. (1988). Análisis Vectorial. Vectores. Vol. 1. Editorial Reverté. Barcelona,

672 Spain. ISBN 84-291-4348-3, pp 162-164. [In Spanish].

673 Shinozaki, K., Yoda, K., Hozumi, K. & Kira, T. (1964). A quantitative analysis of plant.

674 The Pipe Model theory I. *Jpn. J. Ecol*. 14(3): 97-105.

675 Sinoquet, H., Adam, B., Rivet, P. & Godin, C. (1998). Interactions between light and

676 plant architecture in an agroforestry walnut tree, in: Agroforestry Forum, pp. 37-

677 40.

678 Solanelles, F., Escolà, A., Planas, S., Rosell, J.R., Camp, F. & Gràcia, F. (2006). An

679 electronic control system for pesticide application proportional to the canopy

680 width of tree crops. *Biosystems Engineering* 95(4): 473-481.

681 Tarquis, A. & González-Andrés, F. (1995). Stochastic L-system applied to the

682 calculation of the leaf area of a shrubby legume for forage (Chamaecytisus

683 rathenicus, F. ex Wol.). In M. N. Novak (Ed.), Fractal reviews in the natural and

684 applied sciences (pp. 192-203). Chapman and Hall.

685 Tarquis, A.M., Méndez, V., Walklate, P.J., Castellanos, M.T. & Morató, M.C. (2006).

686 L-system tree model and LiDAR simulator: estimation of spray target area.

687 *WSEAS Transactions on Biology and Biomedicine*, 3(2): 81-88.

688 Tourn, G.M., Barthélémy, D. & Grosfeld, J. (1999). Una aproximación a la arquitectura

689 vegetal: conceptos, objetivos y metodología. *Boletín de la Sociedad Argentina de*

690 *Botánica,* 34: 85-99. [In Spanish].

691 Tumbo, S.D., Salyani, M., Whitney, J.D., Wheaton, T.A. & Miller, W.M. (2002).

692 Investigation of laser and ultrasonic ranging sensors for measurements of citrus

693 canopy volume. *Applied Engineering in Agriculture*, 18(3): 367-372.

694 Valentine, H.T. (1985). Tree-growth models: derivations employing the Pipe-model

695 theory. *J. Theor. Biol*. 117(4): 579-585.

696 Von Koch, H. (1905). Une méthode géométrique élémentaire pour l'étude de certaines

697 questions de la théorie des courbes planes. Acta mathematica, 30:145–174.

698 Walklate, P.J., Richardson, G.M., Baker, D.B., Richards, P.A. & Cross, J.V. (1997).

699 Short range LiDAR measurement of top fruit tree canopies for pesticide

700 applications research in the UK. In. Proceedings of SPIE, International Society for

701 Optical Engineering Advances in Laser Remote Sensing for Terrestrial and

702 Oceanographic Application, Orlando, Florida, Vol. 3059 (pp. 143-151).

703 Walklate, P.J., Cross, J.V., Richardson, G.M., Murray, R.A. & Baker, D.E. (2002).

704 Comparison of different spray volume deposition models using LiDAR

705 measurements of apple orchards. *Biosystems Engineering*, 82(3): 253-267.

706 Weber, J. & Penn, J. (1995). Creation and rendering of realistic trees, in: Computer

707 Graphics Proceedings, Annual Conference Series, Acm Siggraph, pp. 381-394.

708   Wei, J. & Salyani, M. (2005). Development of a laser scanner for measuring tree

709   canopy characteristics: phase 2. Foliage density measurement. *Transactions of the*

710   *ASAE*, 48(4): 1595-1601.

711

Table Captions

713   •   **Table 1**. Transition Probability Matrix. The value at line i and column j represents

714   the probability of a transition ($\rho(u)$) from state i to state j. States (u) L, M and S

715   are characterised by a high, medium and low number of metamers per GU,

716   respectively; F stands for presence of flowers. (From Durand et al. 2005, p. 818).

717   •   **Table 2.** Number of internodes used per state, order of the axis and birth year.

718   •   **Table 3.** Succession and branching existence per parent-child state (see Fig. 5 in

719   Durand *et al.*, 2005, p 820).

720   •   **Table 4.** Laser beam starting point (**P**) and laser beam direction (**d**) by type of scan.

721   (x_0, y_0, z_0) is the scanner position which is fixed in all the scanning process.

722   •   **Table 5.** An example of LiDAR simulation to study the sensitivity of the impacted

723   total area in relation to the horizontal resolution (Δy). After the simulation, the user

724   can compare the variation in the impacted area and the error

725

726

Figure Captions

728   •   **Fig. 1**. An example of the use of probability matrix P in succession & branching in

729   different axes of the model for S and M state. A new power of P is used in

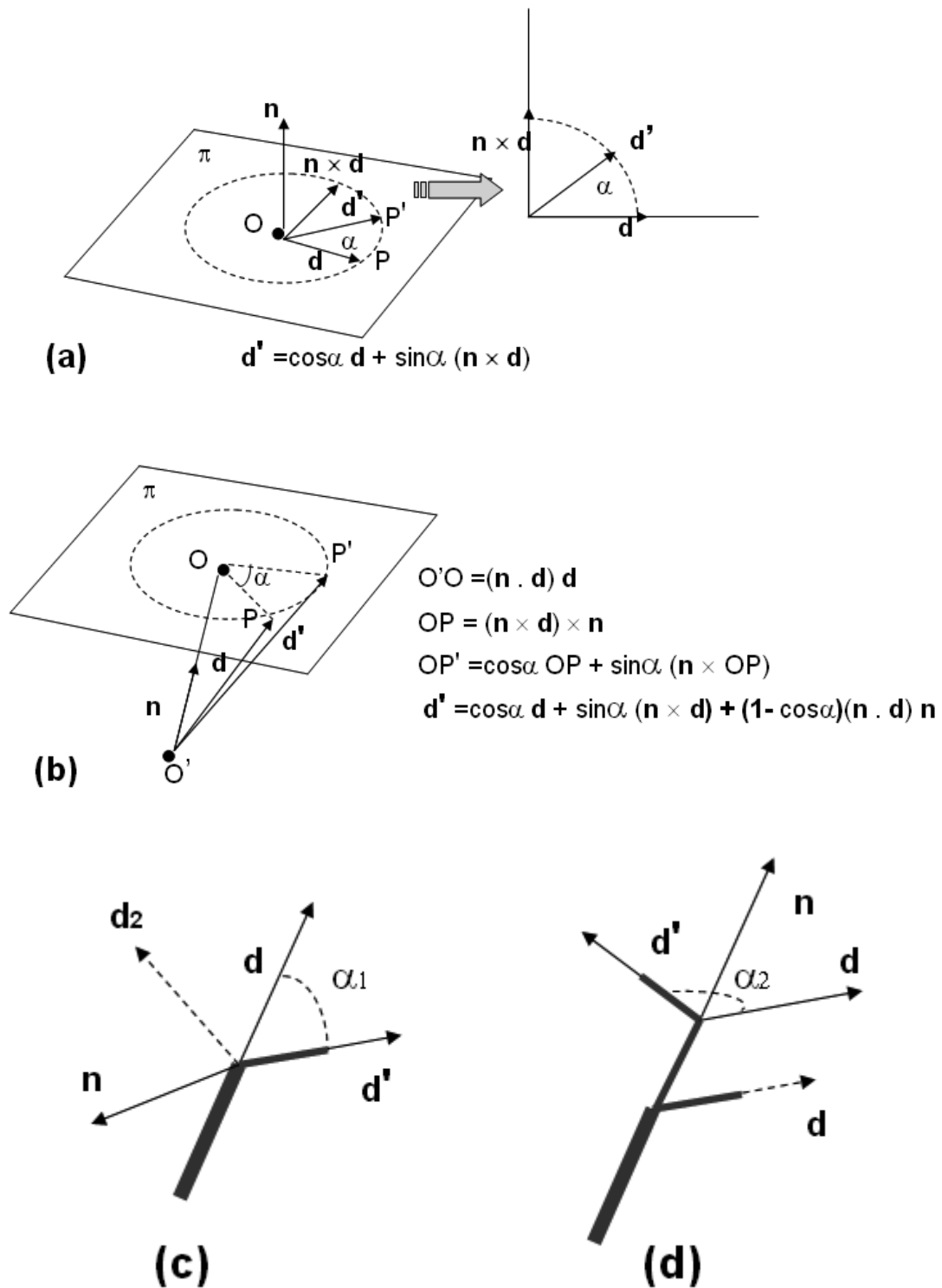730   succession. The original P is recovered in a new branching.

731 • **Fig. 2**. (a) Turning a vector **d** in the plane an angle α. (b) Turning a vector **d** in the

732 space through a direction **n** an angle α. As a result of the turn a new vector **d**$^{'}$ is

733 obtained (Scala, 1988). The turning (b) is applied to branching (c), where an

734 arbitrary direction **d₂** is taken to obtain **n** and a turn of α_1 is done. Subsequently, in

735 the phyllotaxis turning (d), the direction **n** of turn is determined by the axis of the

736 parent branch**.**

737 • **Fig. 3**. An example of a three-dimensional HTM model for apple trees with a

738 number of reiterations equal to 10 and a shady percentage of 80%**.** (a) view of

739 virtual apple tree. (b) lateral angular scan. (c) zenith scan.

740 • **Fig. 4**. Type of scan. Lateral angular (1), opposite lateral angular (2), orthogonal

741 lateral (3), opposite orthogonal lateral (4) and zenith (5).

742 • **Fig. 5**. Calculation of impact (R) of one laser beam in a leaf. P is the scanner origin

743 and Q is an arbitrary point of a polyline that contains the leaf.

744 • **Fig. 6**. An example of a unitary laser beam of I_L - impacted area in foliar layer and

745 I_{3L} - external foliar impacted area**.** The impacted area (I_T) is equivalent to I_L

746 whether the impacted model object is a leaf or a branch.

747 • **Fig. 7**.- **(a)** L_A – Leaf area (dm^2) vs. I_L – Impacted leaf area (dm^2). For lateral

748 scan $L_A = 12.67 \cdot I_L$ with $R^2 = 0.95$ **(a.1)**. For zenith scan $L_A = 7.10 \cdot I_L$ with

749 $R^2 = 0.97$ **(a.2)**. **(b)** L_A – Leaf area (dm^2) vs. I_T – Impacted area (dm^2). For lateral

750 scan $L_A = 8.70 \cdot I_T - 209.15$ with $R^2 = 0.94$ **(b.1)**. For zenith

751 scan $L_A = 6.71 \cdot I_T - 129.84$ with $R^2 = 0.96$ **(b.2)**. **(c)** L_A – Leaf area (dm^2) vs. I_{3L} –

752 Impacted external leaf area (dm^2). For lateral scan $L_A = 6.40 \cdot I_{3L}$ with $R^2 = 0.97$

753 **(c.1)**. For zenith scan $L_A = 3.29 \cdot I_{3L}$ with $R^2 = 0.99$ **(c.2)**.

754

Figure 1
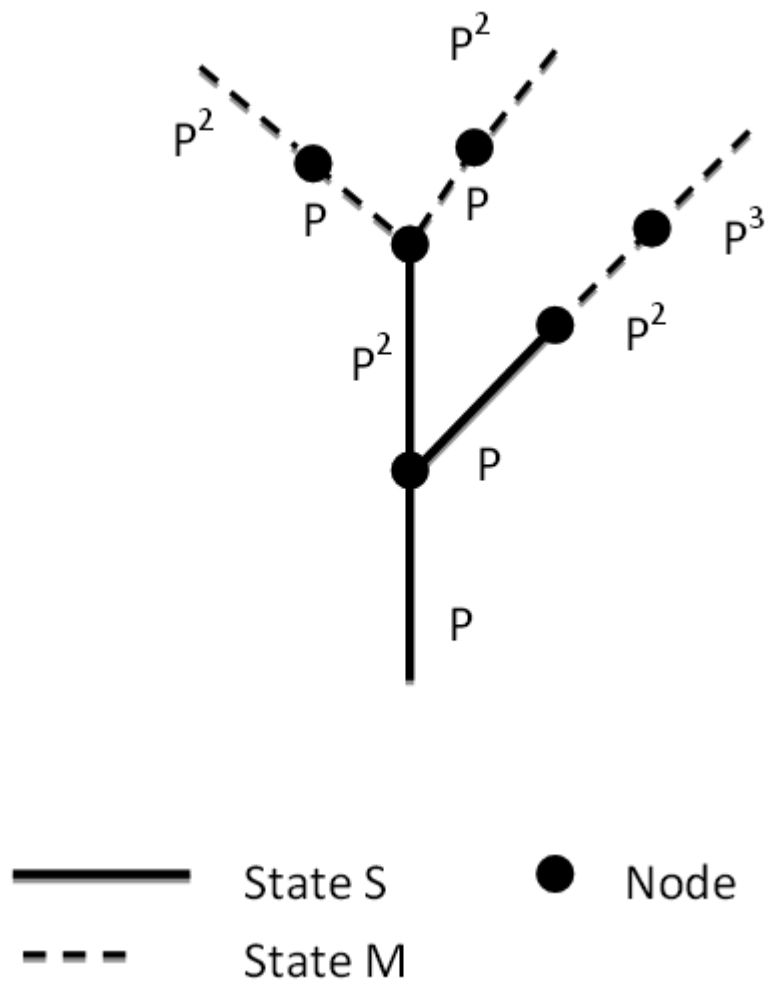
Fig. 1.- An example of the use of probability matrix P in succession & branching in different axes of the model for S and M state. A new potency of P is used in succession. The original P is recovered in a new branching.

Figure 2

(a) $d' = \cos\alpha\ d + \sin\alpha\ (n \times d)$

$O'O = (n \cdot d)\ d$

$OP = (n \times d) \times n$

$OP' = \cos\alpha\ OP + \sin\alpha\ (n \times OP)$

$d' = \cos\alpha\ d + \sin\alpha\ (n \times d) + (1 - \cos\alpha)(n \cdot d)\ n$

Fig. 2.- (a) Turning a vector **d** in the plane an angle α. (b) Turning a vector **d** in the space through a direction **n** an angle α. As result of the turn a new vector **d**' is obtained (Scala, 1988). The turning (b) is applied to branching (c), where an arbitrary direction **d₂** is taken to obtain **n** and a turn of α_1 is done. After, in the phyllotaxis turning (d), the direction **n** of turn is determined by the axis of the parent branch.
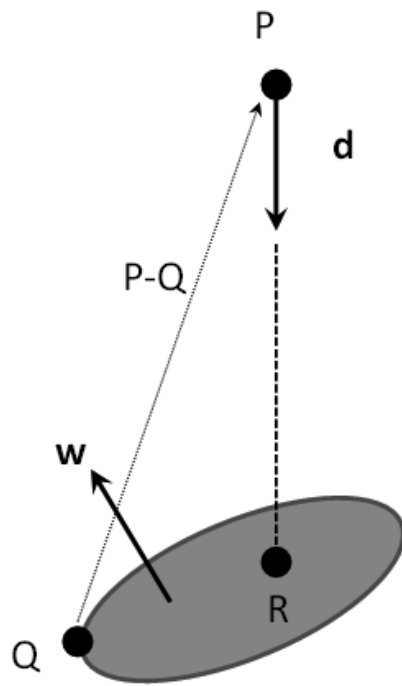
Figure 3

(a)

(b)

(c)
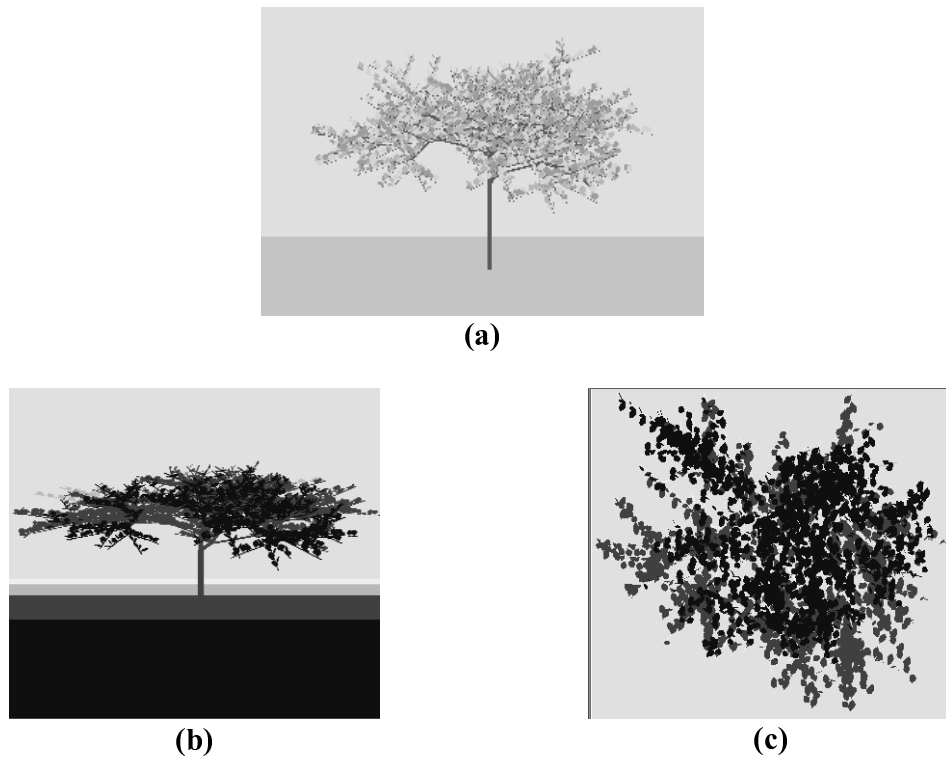
Fig. 3.- An example of a three-dimensional HTM model for apple trees with a number of reiterations equal to 10 and a shady percentage of 80%. (a) View of virtual apple tree. (b) lateral angular scan. (c) zenith scan.

Figure 4
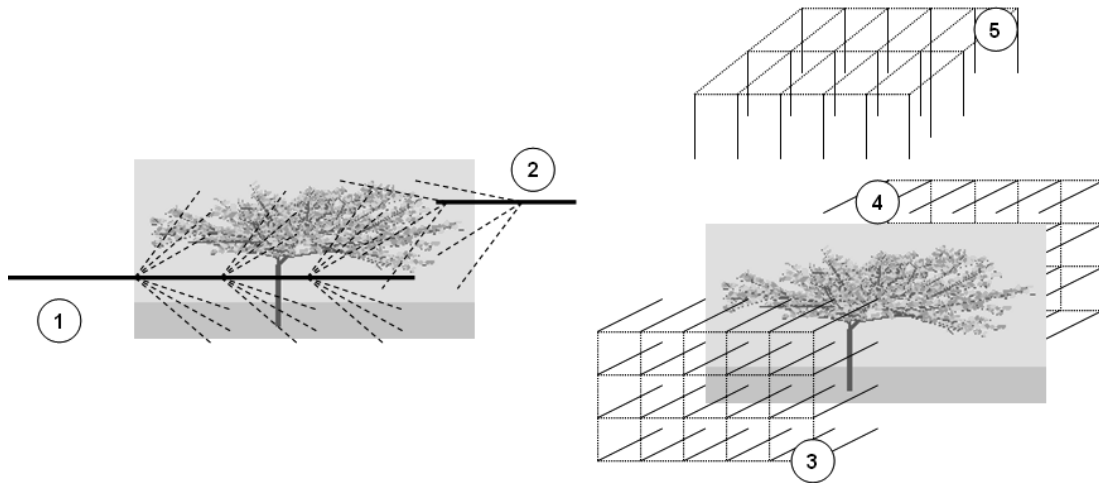
Fig. 4.- Kind of scan. Lateral angular (1), opposite lateral angular (2), orthogonal lateral (3), opposite orthogonal lateral (4) and zenith (5).

Figure 5

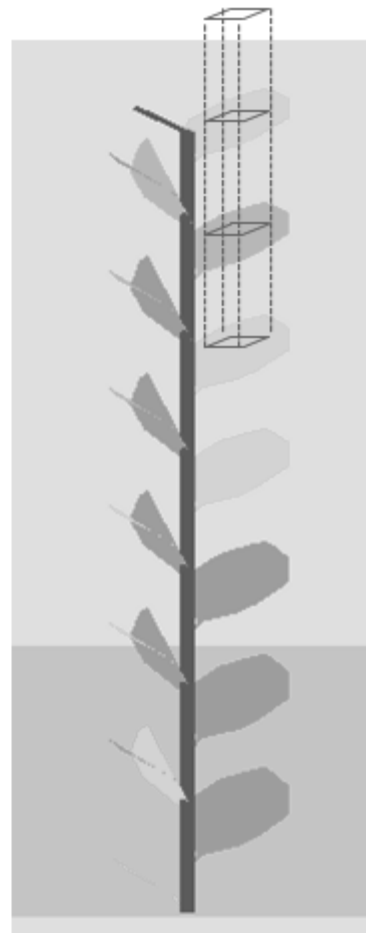(P-Q).**w** : Distance from P to leaf plane

d.w : Modulus of **d** projected over **w**

$\dfrac{(P-Q).\mathbf{w}}{\mathbf{d.w}}$: Scale to use in **d** to impact in leaf plane

Fig. 5.- Calculation of the impact R of one laser beam in a leaf. P is the scanner origin and Q is an arbitrary point of a polyline that contains the leaf.

Figure 6
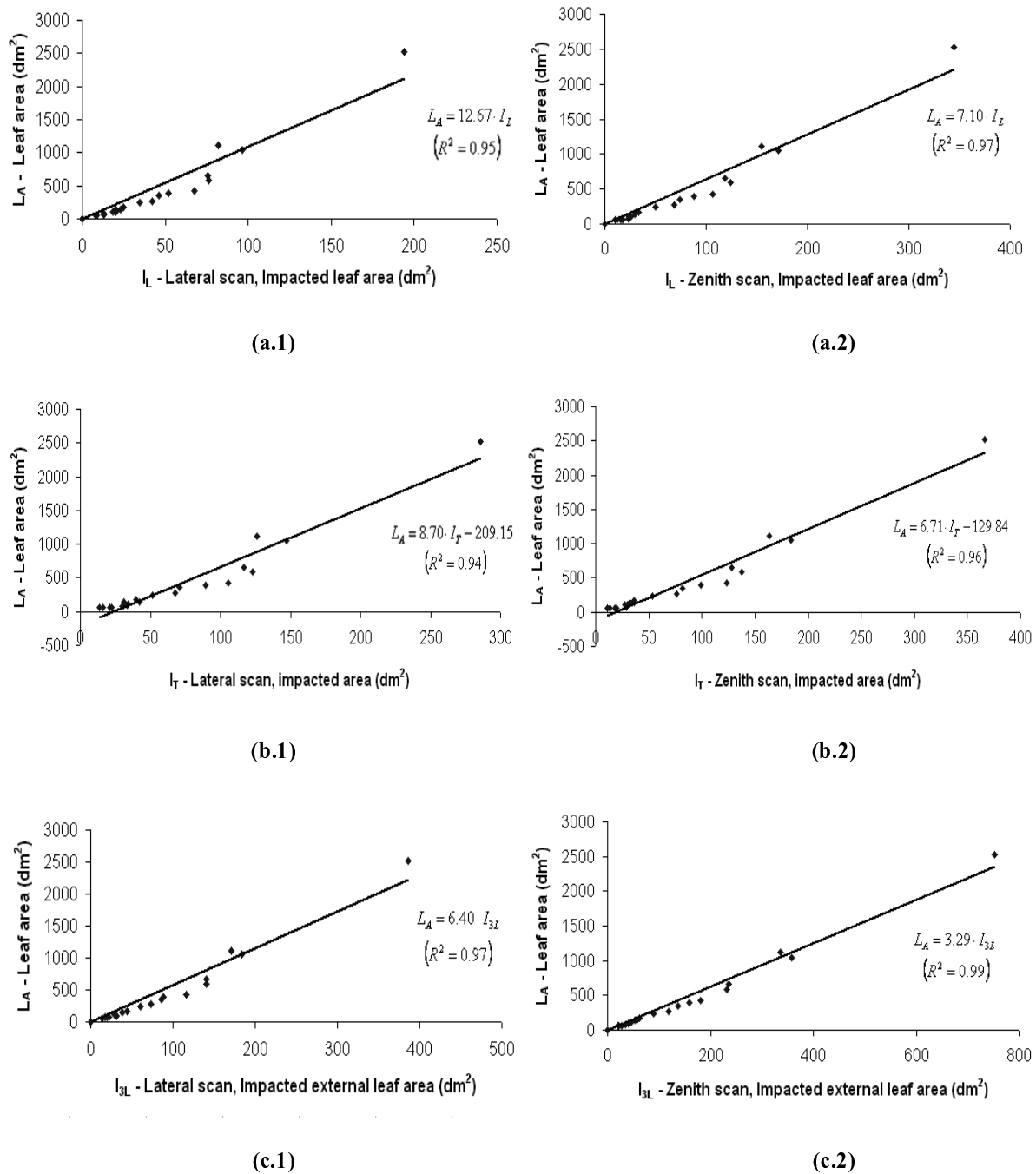

Iʟ – Impacted area in foliage layer for one laser beam

I₃ʟ – External foliage impacted area for one laser beam

Fig. 6.- An example of I_L - impacted leaf area and I_{3L} - impacted area in the three outer leaves. The impacted total area (I_T) is equivalent to I_L whether the model object impacted is a leaf or a branch.

Figure 7

(a.1)

(a.2)

(b.1)

(b.2)

(c.1)

(c.2)

Fig. 7.- (a) L_A – Leaf area (dm^2) vs I_L – Impacted leaf area (dm^2). For lateral scan $L_A = 12.67 \cdot I_L$ with $R^2 = 0.95$ **(a.1)**. For zenith scan $L_A = 7.10 \cdot I_L$ with $R^2 = 0.97$ **(a.2)**. **(b)** L_A – Leaf area (dm^2) vs I_T – Impacted area (dm^2). For lateral scan $L_A = 8.70 \cdot I_T - 209.15$ with $R^2 = 0.94$ **(b.1)**. For zenith scan $L_A = 6.71 \cdot I_T - 129.84$ with $R^2 = 0.96$ **(b.2)**. **(c)** L_A – Leaf area (dm^2) vs I_{3L} – Impacted external leaf area (dm^2). For lateral scan $L_A = 6.40 \cdot I_{3L}$ with $R^2 = 0.97$ **(c.1)**. For zenith scan $L_A = 3.29 \cdot I_{3L}$ with $R^2 = 0.99$ **(c.2)**.

Table 1

u (previous state)	Transition probability matrix $\rho(u)$ – *next state*			
	L	M	S	F
L	0.05	0.15	0.63	0.16
M	0.02	0.06	0.30	0.62
S	0.01	0.05	0.27	0.66
F	0.04	0.35	0.60	0.00

Table 1. Transition Probability Matrix. The value at line *i* and column *j* represents the probability of a transition ($\rho(u)$) from state *i* to state *j*. States (*u*) L, M and S are characterised by a high, medium and low number of metamers per GU, respectively; F stands for presence of flowers. (From Durand et al. 2005, p. 818).

Table 2

State	Order	Year	Internodes
L	1	1	30
L	1	2, 3	25
L	1	≥ 4	20
L	≥ 2	≥ 1	20
M	≥ 1	≥ 1	9
S	≥ 1	≥ 1	1
F	≥ 1	≥ 1	3

Table 2.- Number of internodes used per state, order of the axis and birth year.

Table 3

Parent	Child	Sucession	Branching
L	L	Yes	Yes
L	M	Yes	
L	S		Yes
L	F	Yes	
M	L		
M	M	Yes	
M	S		Yes
M	F	Yes	Yes
S	L		
S	M		
S	S		Yes
S	F	Yes	
F	L		
F	M		Yes
F	S		Yes
F	F		

Table 3.- Succession and branching existence per parent-child state (see Fig 5 in Durand et al., 2005, p 820).

Table 4

Type of scan	P	d
Lateral and angular	$(x_o,\ y_i,\ z_0)$	$(\cos\theta_k,\ 0,\ \sin\theta_k)$
Opposite lateral and angular	$(x_o,\ y_i,\ z_0)$	$(\cos\theta_k,\ 0,\ \sin\theta_k)$
Lateral and orthogonal	$(x_o,\ y_i,\ z_i)$	$(-1,\ 0,\ 0)$
Opposite lateral and orthogonal	$(x_o,\ y_i,\ z_i)$	$(1,\ 0,\ 0)$
Zenital (orthogonal)	$(x_i,\ y_i,\ z_o)$	$(0,\ 0,\ -1)$

Table 4.- Laser beam starting point (**P**) and laser beam direction (**d**) by type of scan. $(x_0,\ y_0,\ z_0)$ is the scanner position which is fixed in all the scanning process.

Table 5

Δy *(mm)*	I_T - *Impacted total area (dm^2)*	$\Delta(I_T)$ *(dm^2)*	*% Error*
2	147.18	0.00	0.0%
3	147.98	0.79	0.5%
4	148.63	1.44	1.0%
5	149.26	2.08	1.4%
6	149.80	2.62	1.8%
7	149.95	2.77	1.9%
8	150.93	3.75	2.5%
10	151.93	4.74	3.2%
15	153.43	6.24	4.2%
20	154.48	7.30	5.0%
25	156.83	9.65	6.6%
35	157.43	10.24	7.0%
40	161.24	14.06	9.6%

Table 5.- An example of LiDAR simulation to study the sensitivity of the impacted total area in relation to the horizontal resolution (Δy). After the simulation, the user can compare the variation in the impacted area and the error.